

Excitation Wavelength-Dependent Upconversion Luminescence Enhancement in Tm^{3+} -Doped $\text{LiErF}_4@ \text{LiYF}_4$ System Under High Pressure

Ling Zhang, Zhongling Lang, Yang Lu, Xu Zhao, Bin Jiang, Xu Yan, Peng Sun, Fengmin Liu, Guangdong Zhou, Mi Zhou, Yanchao Wang, Xiaomin Liu,* and Geyu Lu*

Local structural engineering is an endogenous approach to modulate upconversion luminescence (UCL) from upstream to meet the needs of specific application scenarios. Herein, high pressure is utilized as a means to modulate the local structure, and the designed $\text{LiErF}_4:0.5\%\text{Tm}^{3+}@ \text{LiYF}_4$ (Er:Tm@Y) nanoparticles with fast energy transfer rates, abundant cross-relaxation processes, and multiple near-infrared wavelengths (808, 980, 1530 nm) excitation properties are tailored as local structure-sensitive hosts. A unique excitation wavelength-dependent UCL enhancement of Er:Tm@Y upconversion nanoparticles is observed by pressure-induced local structure distortions. When the pressure of ≈ 6 GPa is applied, the UCL is enhanced by a factor of 2.6 at 980 nm excitation only. After pressure release, the luminescence diminishes and recovers. Density functional theory calculations show that the symmetry distortion of the LiErF_4 crystal reaches a maximum at pressurization to 6 GPa, while a new Er-4f state emerges, greatly reducing the bandgap from 8.3 to 5.7 eV. Comparative experiments demonstrate that the local symmetry distortion caused by $0.5\%\text{Tm}^{3+}$ doping and the different energy transfer patterns of Er^{3+} to Tm^{3+} at different excitations are responsible for this wavelength-dependent luminescence enhancement.

1. Introduction

Photon upconversion luminescence (UCL) is the process in which low-energy excitation (commonly in near-infrared radiation (NIR)) generates high-energy emission via a continuous multiphoton absorption and energy transfer process. Based on this unique optical principle, lanthanide (Ln)-doped upconversion nanoparticles (UCNPs) present their exceptional optical properties such as long lifetime, narrow emission bandwidth, large anti-Stokes shift (several hundred nanometers), deep penetration depth, and superior photostability. These UCNPs already have been applied in diverse fields such as sensing and detection,^[1,2] bioimaging, and diagnostics,^[3–6] photovoltaics and photocatalysis.^[7,8] To meet the different requirements for UCL in various application scenarios, great efforts and various methods have been made, including surface passivation,^[9–11] local structural engineering,^[12,13] excitation power manipulation,^[14] dye sensitization,^[15] and local field effect enhancement,^[16] to obtain UCL with desirable characteristics. Among these methods, local structure engineering is an endogenous approach to UCL from upstream tuning. It is well known that interionic distance, local crystal field strength, and local symmetry play key roles in determining the energy transfer efficiency, energy level splitting, and parity hybridization of Ln^{3+} , respectively.^[12] Therefore, the emission intensity, selectivity, and wavelength shift of UCL can be tuned by local structural engineering.

Pressure is considered as a “clean” means of local structure engineering because it does not introduce other influences into the material. The applied high pressure can cause a series of changes in the physicochemical properties of the material without introducing impurities, including changing the electronic structure, reducing the interatomic/interionic distances, shrinking the lattice volume, and increasing the lattice vibrations (phonon energy) to obtain properties that cannot be observed under conventional conditions, and allowing real-time and reversible tuning of the luminescence. The modulation of local structure-sensitive UCL by high pressure manifests itself in most cases as a quenching of the luminescence, which is due to the increase in phonon energy and cross-relaxation

Pressure is considered as a “clean” means of local structure engineering because it does not introduce other influences into the material. The applied high pressure can cause a series of changes in the physicochemical properties of the material without introducing impurities, including changing the electronic structure, reducing the interatomic/interionic distances, shrinking the lattice volume, and increasing the lattice vibrations (phonon energy) to obtain properties that cannot be observed under conventional conditions, and allowing real-time and reversible tuning of the luminescence. The modulation of local structure-sensitive UCL by high pressure manifests itself in most cases as a quenching of the luminescence, which is due to the increase in phonon energy and cross-relaxation


L. Zhang, Y. Lu, X. Zhao, B. Jiang, X. Yan, P. Sun, F. Liu, X. Liu, G. Lu
State Key Laboratory of Integrated Optoelectronics
College of Electronic Science and Engineering
Jilin University

Changchun 130012, P. R. China
E-mail: xiaominliu@jlu.edu.cn; luyg@jlu.edu.cn

Z. Lang, M. Zhou, Y. Wang
State Key Laboratory of Superhard Materials
Jilin University
Changchun 130012, P. R. China

Z. Lang
Centre for Advanced Optoelectronic Functional Materials Research
Key Laboratory of UV-Emitting Materials and Technology
Ministry of Education
Northeast Normal University
Changchun 130024, P. R. China

G. Zhou
College of Chemistry
Jilin University
Changchun 130021, P. R. China

 The ORCID identification number(s) for the author(s) of this article can be found under <https://doi.org/10.1002/adom.202202884>.

DOI: 10.1002/adom.202202884

(CR) efficiency, and probably higher local symmetry.^[17–20] On the other hand, the reduction of interionic distance and the breaking of local symmetry at high pressure, causing an increase in transition probability and energy transfer efficiency, may lead to the enhanced UCL.^[21,22] However, there are very few relevant reports.

In this work, we purposely tailored the tetragonal phase $\text{LiErF}_4:0.5\%\text{Tm}^{3+}/\text{LiYF}_4$ (abbreviated as Er:Tm@Y) core-shell nanoparticles as local structure-sensitive UCL hosts. It is mainly based on the following considerations: (i) Unlike the case of Yb^{3+} and Er^{3+} codoping, the self-sensitized LiErF_4 system has a fast energy transfer rate and abundant CR processes. (ii) Doping with 0.5% Tm^{3+} impurity may break the local symmetry, and this local symmetry distortion is amplified under high pressure. (iii) By studying the effect of cladding heterogeneous inert shell types including $\text{LiYF}_4/\text{LiLuF}_4/\text{LiGdF}_4$, it facilitates the analysis of the effect of pressure and different interfacial stresses (tensile strain of LiLuF_4 shell and compressive strain of LiYF_4 and LiGdF_4 shell) synergistically modulating the local structure on UCL. (iv) In particular, this material exhibits a unique optical property, multiple NIR wavelength excitations (808, 980, 1530 nm) and near-monochromatic red UCL. The selectable modulation of wavelengths provides a completely new dimension for studying pressure-induced UCL, which has never been addressed in previous studies. The UCL evolution of Er:Tm@Y UCNPs under pressure was investigated in detail. A unique excitation wavelength-dependent enhancement was observed. When the pressure of 6.15 GPa was applied, a 2.6-fold enhancement of UCL was obtained at 980 nm excitation only. After pressure release, the luminescence was restored and the process was reversible. Through further experimental comparative analysis and theoretical simulation calculations, we explored the plausible mechanism for this pressure-stimulated local structural engineering in modulation of UCL. Our work not only opens a new horizon in the understanding of the relationship between local structure and optical performance of UCNPs, but also presents a prospect for exploration of advanced luminescent materials in the future.

2. Results and Discussion

2.1. Structure and Morphology of Er:Tm@Ln UCNPs

Tm^{3+} -doped tetragonal phase LiErF_4 core UCNPs with a doping concentration of 0.5% were prepared by the classical high-temperature solvothermal approach.^[23] Our previous studies have demonstrated that the $\text{LiErF}_4:0.5\%\text{Tm}^{3+}$ (abbreviated as Er:Tm) core is nonluminescent owing to concentration quenching effects.^[24] Shelling is a commonly adopted strategy to enhance the intensity of UCNPs by passivating the surface defects and thereby eliminating concentration quenching.^[25,26] It is crucial to decide which types of shell materials as it affects the growth, optical properties, and compatibility towards the extrinsic environment of the UCNPs.^[27–30] Figure 1a indicates the construction of the core-shell structure of $\text{LiErF}_4:0.5\%\text{Tm}^{3+}/\text{LiLnF}_4$ (abbreviated as Er:Tm@Ln, Ln = Y, Lu, Gd), clarifying the influence of the heterogeneous LiLnF_4 (Ln = Y, Lu, Gd) shell on the Er:Tm core. Since LiGdF_4 and LiYF_4 have large lattice

constants, they must be compressed to match the Er:Tm core, whereas LiLuF_4 undergoes tension. First, 2 mmol of Er:Tm core UCNPs were synthesized which enabled all shells to be epitaxially grown on the same core, allowing for a more accurate comparison among core-shell UCNPs. The average diameter of the core was $(28.3 \pm 1.0) \times (18.5 \pm 1.0)$ nm (Figure S1, Supporting Information). The TEM images in Figure 1b–d exhibit the monodispersity of tetragonal bipyramidal core-shell UCNPs, which have a mean dimension of $(35.1 \pm 1.4) \times (23.0 \pm 1.3)$ nm (Er:Tm@Y), $(32.0 \pm 1.2) \times (20.6 \pm 1.2)$ nm (Er:Tm@Lu), and $(30.2 \pm 1.6) \times (25.2 \pm 1.2)$ nm (Er:Tm@Gd), respectively. The high-resolution TEM images in the inset of Figure 1b–d indicate clear lattice fringes with a d -spacing of 0.47 nm for the UCNPs, corresponding to the (101) crystal plane of LiErF_4 , confirming the high crystallinity of the prepared UCNPs. The elementary mapping of Er, Tm, and Y/Lu/Gd demonstrates that Er and Tm are located inside the UCNPs and Y/Lu/Gd is successfully coated externally (Figure S2, Supporting Information).

To investigate the effect of heterogeneous shelling on the structure, X-ray diffractometer (XRD) was used to characterize the structural properties of UCNPs. As shown in Figure 2a, XRD patterns of UCNPs are well matched to the standard tetragonal phase LiErF_4 (JCPDS. No. 51–1618). Meanwhile, a more detailed analysis of single diffraction peaks such as zoom-in of the (101) crystal plane indicates that the peak of Er:Tm@Lu UCNPs shifts toward a larger 2θ angle, while smaller 2θ angles for Er:Tm@Gd UCNPs, as shown in Figure 2b. The smaller 2θ angle is correlated with a larger d -spacing, corresponding to a 4.3% larger ionic radius for Gd^{3+} than for Er^{3+} . The converse is also valid for Lu^{3+} with a 2.4% mismatch. However, the relatively minor difference in radius mismatch (1.3%) between the Y^{3+} and Er^{3+} leads to no significant shift for 2θ , as shown in Figure 2e.

2.2. Luminescence Properties of Er:Tm@Ln UCNPs Under Ambient Conditions

Besides structural changes, shelling also has a significant effect on the optical properties of the UCNPs. Figure 3a and Figure S3 (Supporting Information) illustrate the steady-state UCL spectra of Er:Tm core and Er:Tm@Ln (Ln = Y, Lu, Gd) core-shell UCNPs under ambient conditions at 980, 808, and 1530 nm excitation. The results show that the Er:Tm core UCNPs exhibits almost no emission and a bright near-monochromatic red emission was obtained from the Er:Tm@Ln (Ln = Y, Lu, Gd) core-shell UCNPs via the LiLnF_4 (Ln = Y, Lu, Gd) shelling. The red (640–680 nm) and green (510–560 nm) emissions are assigned to $^4\text{F}_{9/2} \rightarrow ^4\text{I}_{15/2}$ and $(^2\text{H}_{11/2}, ^4\text{S}_{3/2}) \rightarrow ^4\text{I}_{15/2}$ of Er^{3+} , respectively. Notably, LiYF_4 yields a brighter UCL as an inert shell over LiGdF_4 and LiLuF_4 . Furthermore, the temporal behaviors of red ($\text{Er}^{3+}: ^4\text{F}_{9/2} \rightarrow ^4\text{I}_{15/2}$, 668 nm) and green ($\text{Er}^{3+}: ^4\text{S}_{3/2} \rightarrow ^4\text{I}_{15/2}$, 550 nm) emissions of these three Er:Tm@Ln (Ln = Y, Lu, Gd) core-shell UCNPs at 980 nm excitation were also measured, as shown in Figure 3b,c. Their decay times of $^4\text{F}_{9/2} \rightarrow ^4\text{I}_{15/2}$ are 102.1, 30.5, and 34.1 μs , respectively, indicating that the Er:Tm@Y UCNPs possess the longest lifetime, which is in agreement with the trend of the steady-state UCL spectra. Likewise, the decay times of $^4\text{S}_{3/2} \rightarrow ^4\text{I}_{15/2}$ are 45.3, 20.5, and 29.4 μs , respectively. In Figure S4 (Supporting Information),

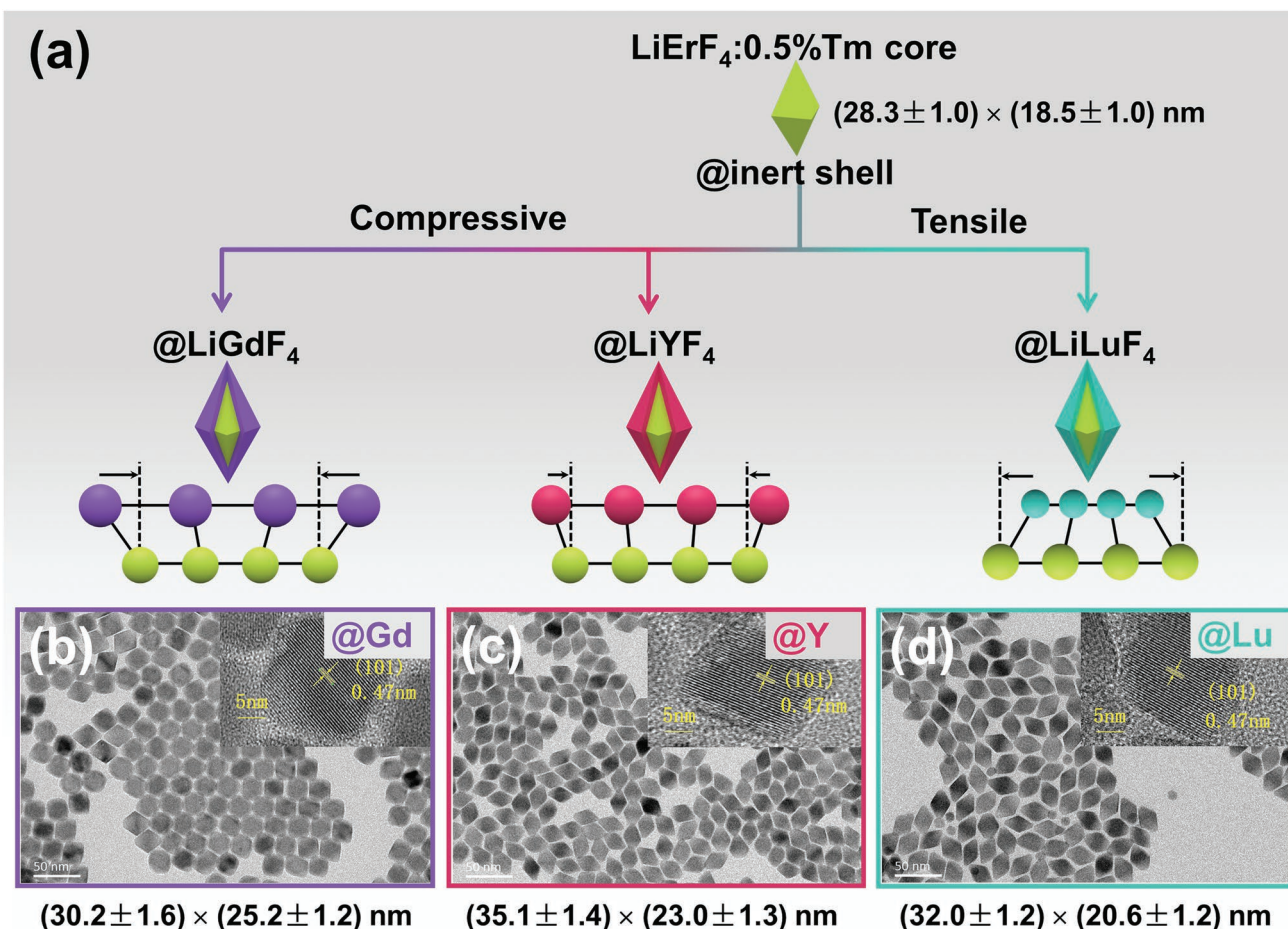


Figure 1. Scheme and images of core-shell UCNPs. a) Three types of inert shell materials including LiYF_4 , LiLuF_4 , and LiGdF_4 are employed to coat the same Er:Tm bare core to obtain the brightest UCL; b–d) TEM images show the tetragonal bipyramidal morphology and monodispersity of synthesized core-shell UCNPs.

lifetime curves for red and green emission states at 808 and 1530 nm excitation were also included, which emphasize similar trends. These results suggest that LiYF_4 shelling presents the greatest UCL performance among these three inert shell materials for Er:Tm core. To explain the reason, we compared the standard lattice constants of LiLnF_4 ($\text{Ln} = \text{Y}, \text{Lu}, \text{Gd}$) with LiErF_4 , as shown in Figure 2c,d. The correlated mismatches to the LiErF_4 in lattice constant a are 0, -0.813% , and $+0.813\%$, respectively. In addition, the correlated mismatches to the LiErF_4 in lattice constant c are 0.002% , -0.016% , and $+0.027\%$, respectively. Consequently, the LiYF_4 shell has the smallest lattice mismatch to LiErF_4 out of these heterogeneous shell materials. Therefore, the LiYF_4 shelling is closest to homogeneous epitaxial growth, resulting in the minimal interface defects and the brightest UCL. In the following, we took Er:Tm@Y UCNPs as the object to investigate their UCL properties under high pressure.

2.3. Modulation of Er:Tm@Y UCL by Pressure-Stimulated Local Structural Engineering

Next, we conducted an optical test on the brightest Er:Tm@Y UCNPs under variable pressures. A diamond anvil cell (DAC)

for producing high pressure coupled to a 980 nm laser was built for in situ UCL measurements, as shown in Scheme 1. The UCL spectra under compression (0–12.90 GPa) are shown in Figure 4a, where the UC luminescence intensity of Er:Tm@Y UCNPs is significantly enhanced under high pressure compared to ambient condition (0 GPa). Also, as the pressure increases, both the overall UCL intensities show a trend of first increasing and then slightly decreasing. Sequential calculations demonstrate a 2.6-fold enhancement for integrated UCL intensity (Figure 4b) at an exerted pressure of 6.15 GPa, in contrast to most other cases where UCL intensity of upconversion materials undergoes quenching under high pressure.^[17,19,29,31] Although gradually becomes weakened, the absolute UCL intensity of Er:Tm@Y UCNPs measured at 6.15–12.90 GPa is still higher than (more than twofold) that recorded under ambient conditions (0 GPa).

In the pressure range of 0–12.90 GPa, the emission band centroids corresponding to the energy transition of $^4\text{S}_{3/2} \rightarrow ^4\text{I}_{15/2}$ and $^4\text{F}_{9/2} \rightarrow ^4\text{I}_{15/2}$ of Er:Tm@Y UCNPs were red-shifted from 548.5 to 551.6 nm, and 665.8 to 670.3 nm, respectively, at 980 nm excitation (Figure 4c; Figure S5, Supporting Information). The local lattice distortion increases the splitting of multiplets during compression, and the energy level gap

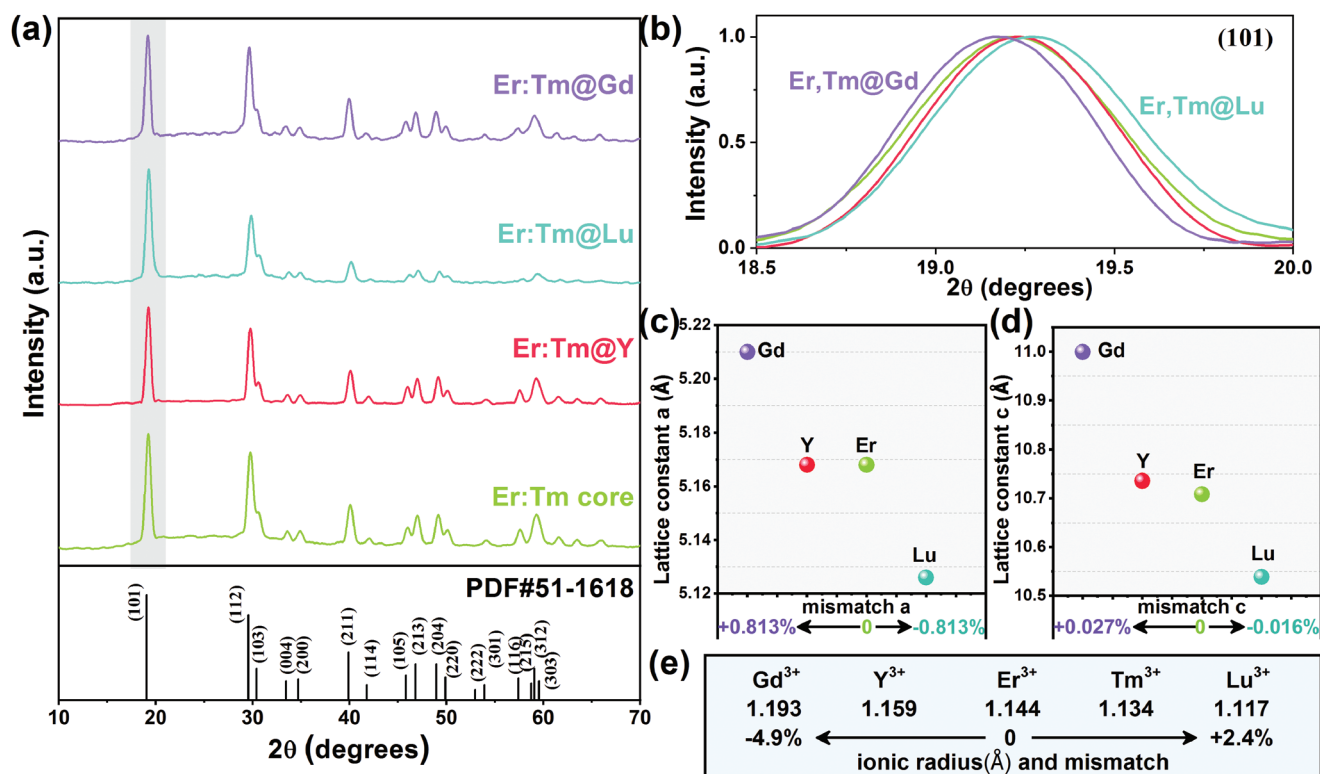


Figure 2. Structural characterization. a) XRD peaks for core and core-shell UCNP; b) A zoom-in of the (101) diffraction peak shows a shift in the 2θ angle position; c,d) Standard lattice parameters of LiLnF₄ (Ln = Er, Y, Lu, Gd); e) The ionic radii of Ln³⁺.

between the ground (⁴I_{15/2}) and excited states (⁴S_{3/2}, ⁴F_{9/2}) of Er³⁺ decreases, leading to the UCL peaks being red-shifted and broadened (Figure 4d).^[12]

Pressure-induced UCL enhancement and red-shift were also observed for Er:Tm@Lu and Er:Tm@Gd at 980 nm excitation similar to that of Er:Tm@Y (Figure S6, Supporting Information). The lattice mismatch between the LiYF₄ shell and LiErF₄ is minimal. The radii of Gd³⁺ and Y³⁺ are larger than that of Er³⁺, the shell layer needs to be compressed to match the bare core, and the interface exhibits compressive stress. Conversely, the radius of Lu³⁺ is smaller than the Er³⁺, the shell layer needs to be stretched to fit the bare core, and the interface exhibits tensile stress (Figure 1a). From the evolution of the

pressure-induced UCL spectra of the above three types of core-shell UCNP, the differences in the degree of luminescence enhancement and the red-shift of the spectral positions are not significant (Figure 4a,c; Figure S6, Supporting Information). This indicates that different interfacial stresses under applied pressure have little effect on the UCL properties of the tetragonal phase Er:Tm core, implying that the pressure dominates the modulation of the local structure compared to the interfacial stress.

We thereafter measured the UCL over two complete cycles of compression and release from ambient condition to high pressure (10.50 GPa/11.94 GPa), as shown in Figure 5. In each cycle, the intensity of the UCL tends to increase with increasing

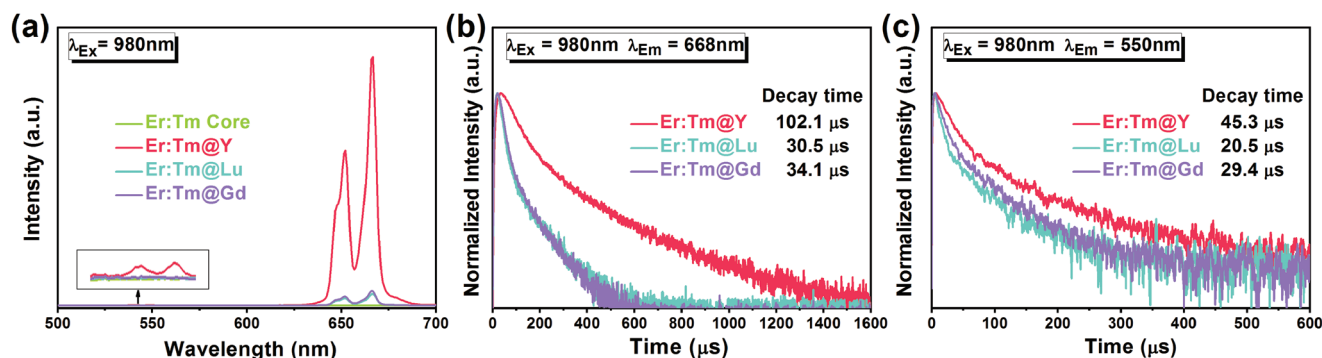
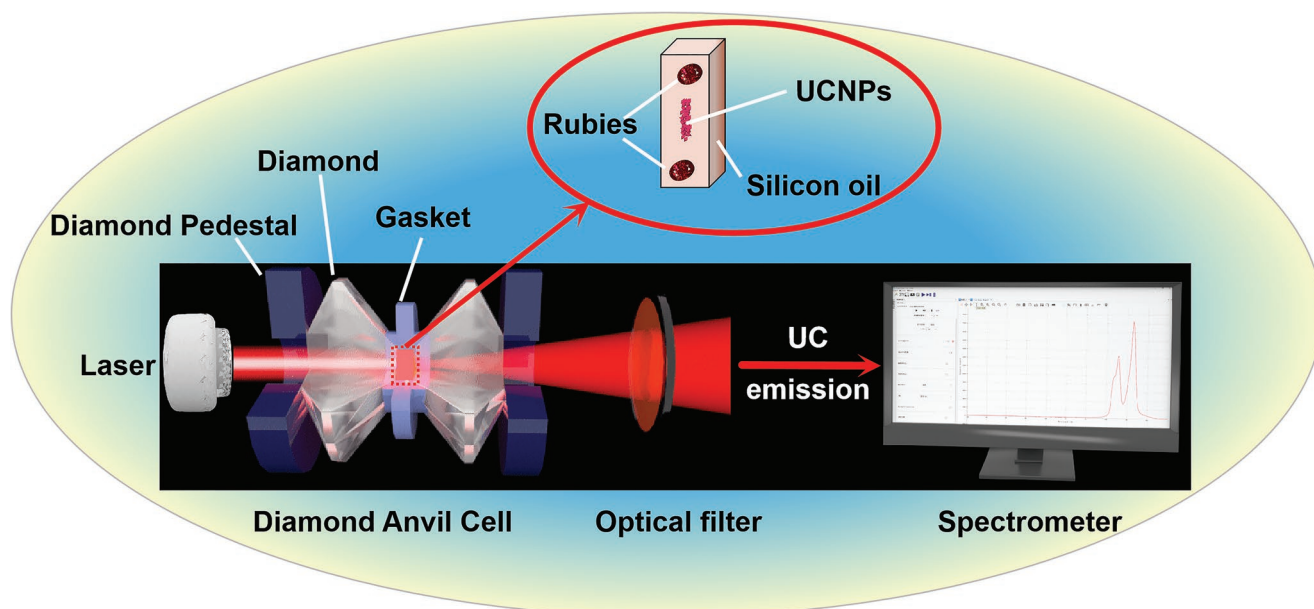


Figure 3. UCL properties. a) UCL spectra of core and core-shell UCNP under ambient conditions at 980 nm excitation (1.05 W); Lifetime curves of b) red emission (668 nm) and c) green emission (550 nm) for various UCNP at 980 nm excitation.



Scheme 1. Schematic diagram of experimental DAC design for detecting the UCL of Er:Tm@Y UCNPs under high pressure. The enlargement on the top shows the central hole of the gasket filled with rubies for pressure calibration, sample (UCNPs) and a pressure-transmitting medium (silicon oil), a filter eliminates signal from the laser source, and the spectra of UCL are recorded by a spectrometer.

pressure and then slightly decreases but is also stronger than the intensity at 0 GPa. Moreover, after the first cycle of compression and release under high pressures, the UCL intensity of the Er:Tm@Y UCNPs remains enhanced for the second

cycle with pressures ranging from 0 to 11.94 GPa (Figure 5a). It indicates that the crystal structure is not destroyed after the pressure release and the original coordination environment of the luminescent ions can be retained. The modulating effect of

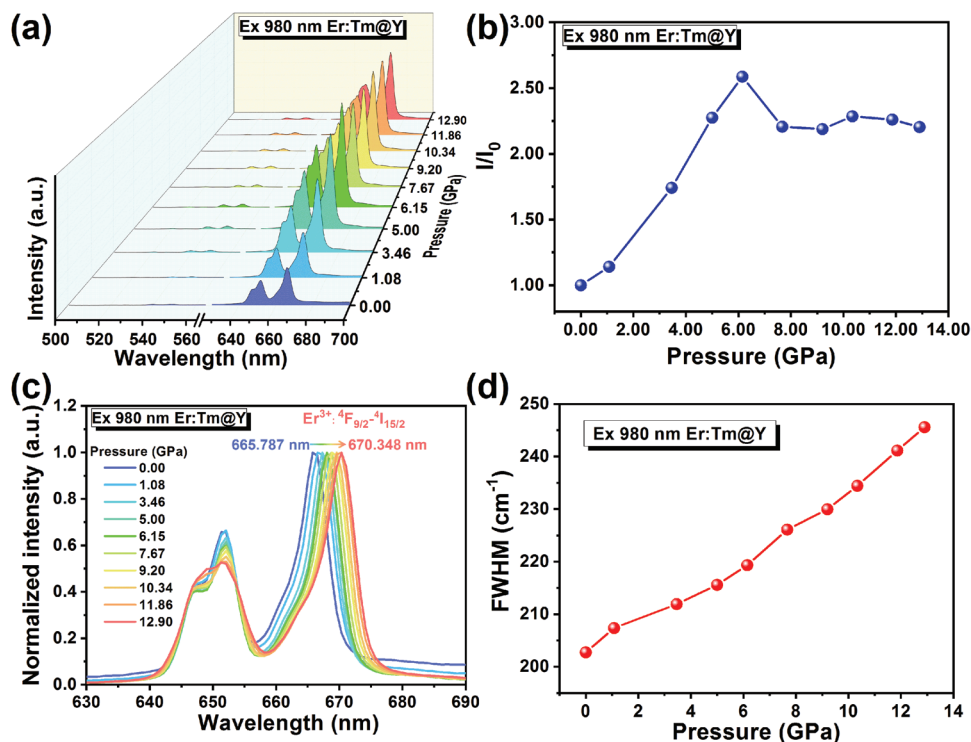


Figure 4. The UCL performance of Er:Tm@Y UCNPs under pressure. a) Pressure-response UCL spectra and b) pressure-dependent overall integrated emission intensity evolution at 980 nm excitation (1.17 W) for the Er:Tm@Y UCNPs; Normalized emission spectra of c) ${}^4F_{9/2} \rightarrow {}^4I_{15/2}$ for the Er:Tm@Y UCNPs; d) FWHM of Er:Tm@Y UCL bands corresponding to ${}^4F_{9/2} \rightarrow {}^4I_{15/2}$ energy transitions as a function of increased pressure.

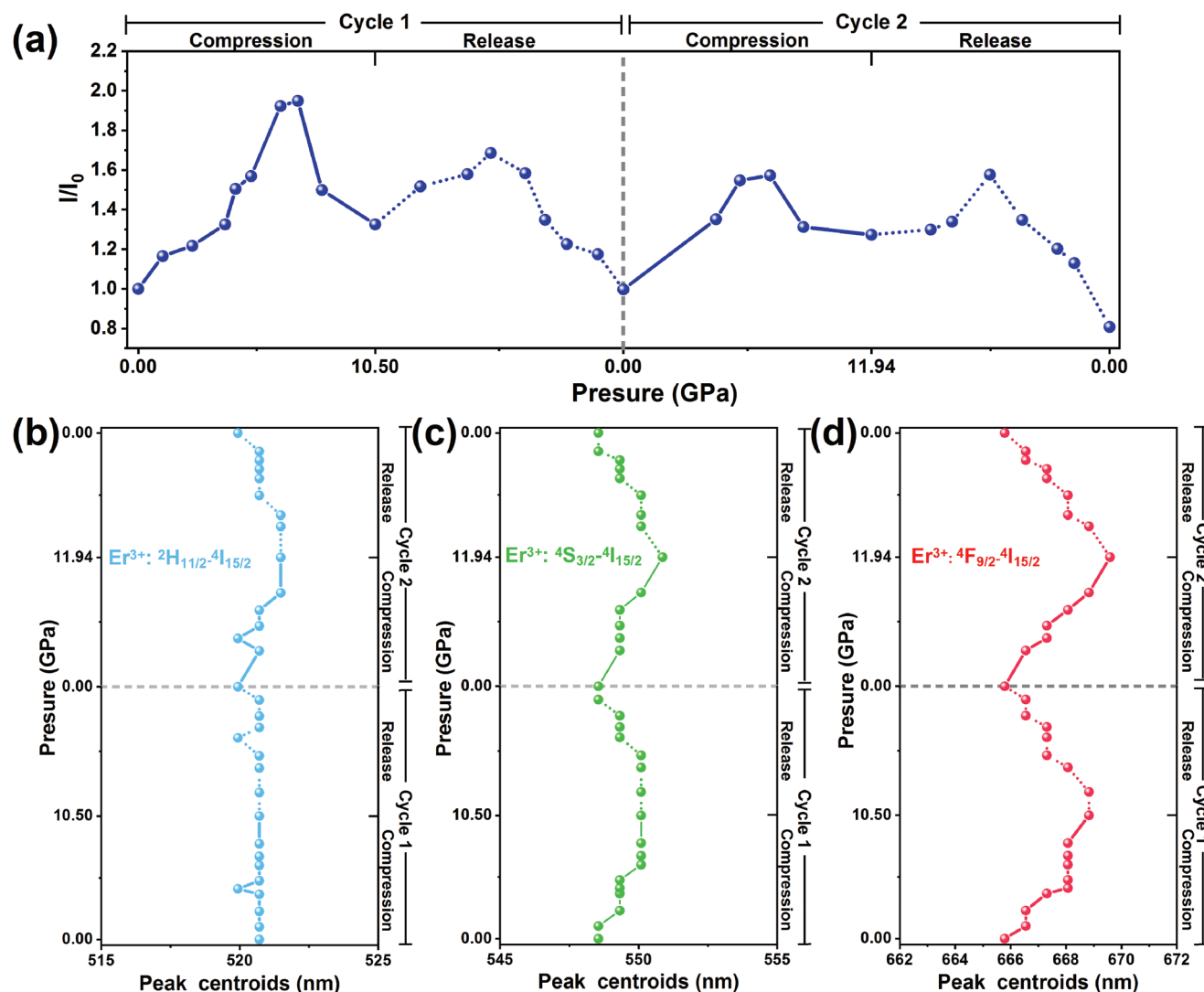


Figure 5. DAC measurements over two complete compression and release cycles for Er:Tm@Y UCNP at 980 nm excitation (2.55 W); a) The overall intensity of UCL; Evolution of the centroids of Er:Tm@Y UCL bands corresponding to the transitions of b) $2H_{11/2} \rightarrow 4I_{15/2}$, c) $4S_{3/2} \rightarrow 4I_{15/2}$, and d) $4F_{9/2} \rightarrow 4I_{15/2}$.

pressure on the local structure is reversible. It should be noted that during the compression–release cycle, crystal defects are created which can permanently quench part of the emitting center, resulting in a slight irreversible weakening of the emission intensity.^[19,22] Besides, for each cycle, when the exerted pressures are released, the emission bands exhibit blue-shift. Correspondingly, the shift of the emission band centroids is approximately symmetrical during pressure release to that in compression (Figure 5b–d dotted line), suggesting that the changes in the interionic distances are reversible during the compression–release cycle.

2.4. Mechanism of Luminescence Enhancement of Er:Tm@Y UCNP at 980 nm Excitation Under High Pressure

To further reveal the mechanism of pressure-induced emission enhancement of Er:Tm@Y UCNP, in situ high-pressure

Raman spectra of Er:Tm@Y UCNP powder in the DAC system were measured via a Raman spectrometer with 532 nm excitation (output power, 10 mW), as shown in Figure 6a. Under ambient conditions, there are main four Raman peaks located at 295, 325, 351, and 406 cm^{-1} in the range of 100–500 cm^{-1} (Figure 6b). The LiLnF_4 (Ln = Er, Y, Lu, Gd) structure is iso-morphous with tetragonal scheelite (CaWO_4) and belongs to the $I4_1/a$ space group symmetry.^[32,33] Each structural unit contains a Y bonded to a tetrahedron, which consists of a Li atom in the center and four F atoms around it (Figure 6c). The internal binding of the $[\text{LiF}_4]^{3-}$ tetrahedra is not significantly different from the other ionic forces in the crystal, so that the internal and external vibrations cannot be well separated in Raman spectra. Therefore, it is difficult to assign a definite atomic motion to any particular mode.^[34] The determined pressure dependence of the frequency values (peak centroids) in the pressure range from 0 to 12.61 GPa is presented in Figure 6d. The Raman spectra of Er:Tm@Y UCNP demonstrate that

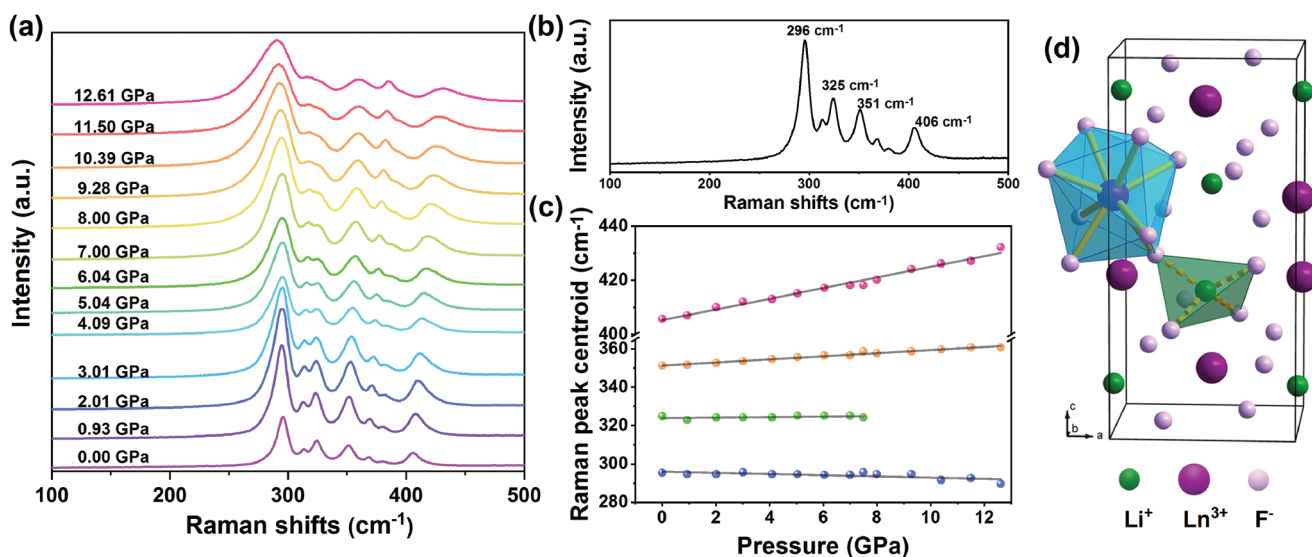


Figure 6. Raman spectra of Er:Tm@Y UCNPs under a) various pressure (0–12.61 GPa) and b) ambient condition; c) The pressure dependence of Raman active phonon frequencies of Er:Tm@Y UCNPs (Solid lines are linear fits giving $\partial\nu/\partial P$); d) Tetragonal unit-cell of LiLnF₄ (Ln = Er, Tm, Y, Lu, Gd).

the characteristic phonon bands located at 351 and 406 cm⁻¹ gradually shift to 361 and 432 cm⁻¹, respectively. This phonon bands blue-shift was due to the shorter interionic distance of the structure in compression and thus the energy of the lattice mode phonons increased. In parallel, no abrupt changes in frequencies (frequency discontinuities) or new Raman bands were observed in compression, implying the absence of crystal structure phase transition, and consequently the UCL enhancement due to the phase transition at high pressure is excluded.

We further performed a series of density functional theory (DFT) calculations using LiErF₄ crystals as a model to examine the pressure-induced changes in their structure and energy bands. The dependencies of the geometric and electronic properties versus the pressure are mainly discussed. **Figure 7a,b** shows the lattice constant changes (*a* and *c*) from 0 to 10 GPa. The lattice constant *a* decreases monotonically as pressure is applied uniformly, while the *c* shows a small platform with external pressure at around 6 and 10 GPa. This means that when the pressure reached at 6 GPa, it will mainly affect the ion

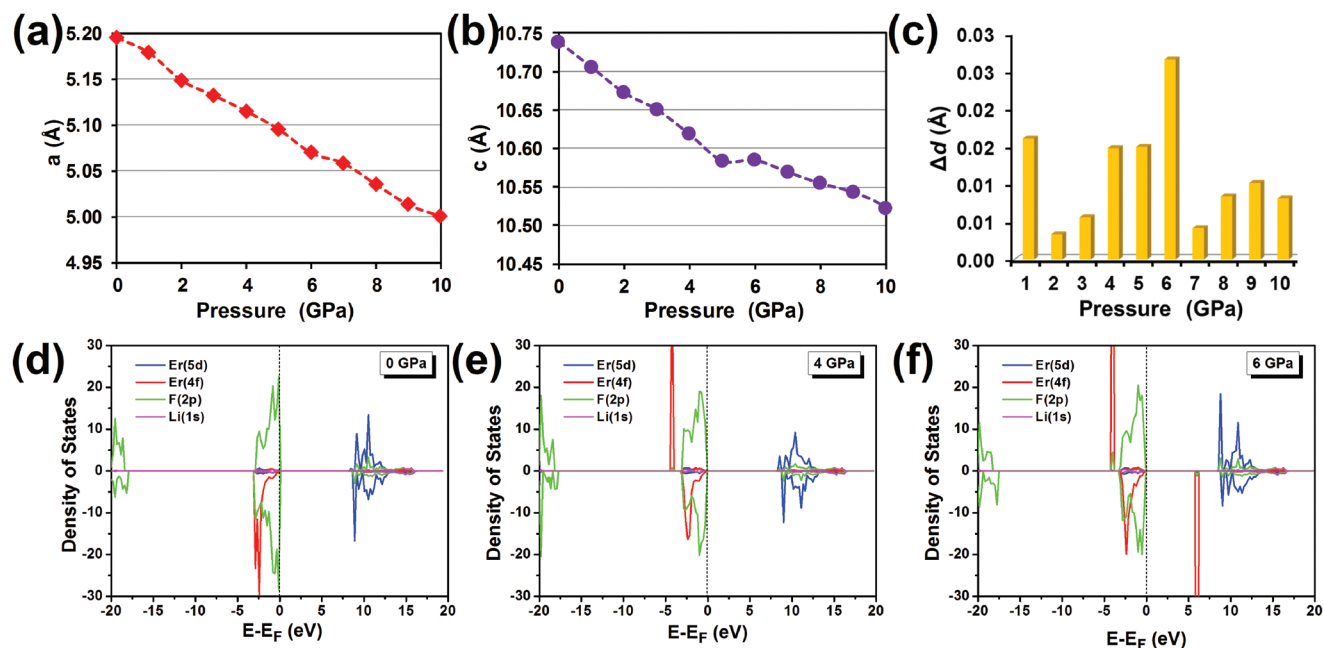


Figure 7. DFT calculations. a,b) Lattice constant-pressure curves for the LiErF₄ crystal in *a*- and *c*-axis; c) symmetry distortion degree between *a*- and *c*-axis ($\Delta d = |(a_{p+1} - a_p) - (c_{p+1} - c_p)|$), *P* is the uniform pressure (change every one GPa) applied on the crystal; d–f) the simulated PDOS for LiErF₄ under the pressures of 0, 4, and 6 GPa (the results of 8 and 10 GPa are presented in Figure S7 in the Supporting Information).

bond along the *a*-axis while having no obvious effect on the *c* direction. To evaluate the different compression behavior along with the *a* and *c* axis, the constant change difference between them is presented in Figure 7c. We can see at around 6 GPa, the change differences between *a* and *c* exhibit the greatest values, resulting in relatively large symmetry distortion of the LiErF₄ crystal. The distortion of the crystal may increase the energy transition probability and thus improve luminescence intensity. This is consistent with our experimental observation that the UCL enhancement is maximum at ≈6 GPa. To understand the electronic character under different pressures in more detail, we compared the partial-projected density of states (PDOS) for the individual atomic contributions to the valence and conduction bands under pressures of 0, 4, and 6 GPa, respectively, as shown in Figure 7d–f. Without any external pressure, the conduction region is mainly dominated by Er-5d states, while the frontier of the valence region is contributed by F-2p states. In addition, the Er-4f states are found to hybridize with the F-2p electron and exhibit a doublet peak at around –2.5 eV below the valence band maximum (VBM). By increasing the pressure to 4 GPa, we see a splitting of Er-4f states and spin-flip from down to up with respect to 0 GPa. Interestingly, a new Er-4f state is inserted between the occupied F-2p and unoccupied Er-5d upon pressure application to 6 GPa, significantly decreasing the bandgap from 8.3 to 5.7 eV. The new existing Er-4f state may induce some new transitions that are related to the luminescence process, and this further verifies that the UCL is at its strongest at ≈6 GPa.

Only lattice distortion and energy band change are not sufficient to cause the enhancement of luminescence, because our comparative study revealed that achieving enhanced UCL also depends on doping. We comparatively measured the in situ pressure-induced UCL spectra of LiErF₄@LiYF₄ (abbreviated as Er@Y) without Tm³⁺ doping at 980 nm excitation, as shown in Figure 8a. With increasing pressure, the emission peaks were red-shifted (Figure S8a, Supporting Information), but the UCL diminished. We suggest that this pressure-induced UCL enhancement of Er:Tm@Y UCNP is largely ascribed to pressure-stimulated distortions in the centrosymmetric environment of the Er³⁺. Electric dipole transitions between states with the same parity are forbidden by the Laporte selection rules, even if such transitions do occur, the intensity is relatively low.^[21] In a relatively ideal crystal (Er@Y), the high pres-

sure only shortens the bond length, and thus the lattice phonon energy increases, while the coordination-environment symmetry remains unaffected. As a result, the increase in phonon-assisted nonradiative relaxation and cross-relaxation leads to a decrease in the UCL of Er@Y UCNP. However, in the case of the doped Er:Tm@Y UCNP, the local geometry around the Er³⁺ is inhomogeneous and intensifies at high pressures, which leads to an increase in transition probability.^[21] Specifically, in previous studies, the use of Tm³⁺ dopants as trapping centers for excitation energy could reduce the luminescence quenching effects by preventing the energy migration in the host lattice.^[24,26] During the compression process, the distance between Er³⁺ and Tm³⁺ is shortened, the coupling between ions is strengthened, and the energy transfer rate is accelerated, which is more favorable for Tm³⁺ to play the role of storing excitation energy and reducing the migration-mediated energy loss in the lattice, resulting in the enhanced UCL.^[19]

Based on the property that Er:Tm@Ln (Ln = Y, Lu, Gd) can be excited at multiple NIR wavelength (808, 980, 1530 nm) excitations, we introduced the wavelength as a dimension of variation for the first time in the pressure-induced luminescence study. It is interesting to find that the pressure-induced UCL enhancement in Er:Tm@Y was not observed at 1530 and 808 nm excitation, but the red-shift of the emission peak is present, as shown in Figure 8b,c and Figure S8b,c (Supporting Information). This is because the transfer of energy from Er³⁺ to Tm³⁺ under excitations at 808 and 1530 nm requires filling from the ⁴I_{9/2} state to the ⁴I_{11/2} state, a process that needs phonon-assisted nonradiative relaxation, as shown in Figure 9a,b. The increase of lattice phonon energy in compression could affect the non-radiative transition process from ⁴I_{9/2} to ⁴I_{11/2}, which in turn affects the population of Er³⁺ on the ⁴I_{11/2} energy level. The energy transfer process from Er³⁺ to Tm³⁺ is suppressed, resulting in more energy being dissipated. Eventually, the excitation energy captured by the Tm³⁺ decreases, and the luminescence is diminished. In contrast, at 980 nm excitation, the photons are directly populating the ⁴I_{11/2} state without the non-radiative transition from ⁴I_{9/2} to ⁴I_{11/2}, thus exhibiting enhanced UCL (Figure 9c). The red-shift and broadening of Er:Tm@Lu and Er:Tm@Gd UCNP in the UCL band at 808 and 1530 nm excitation are similar to those of Er:Tm@Y UCNP, but no pressure-induced enhancement of UCL is also observed (Figures S9 and S10, Supporting Information). To sum up, Er:Tm@Ln (Ln = Y, Lu,

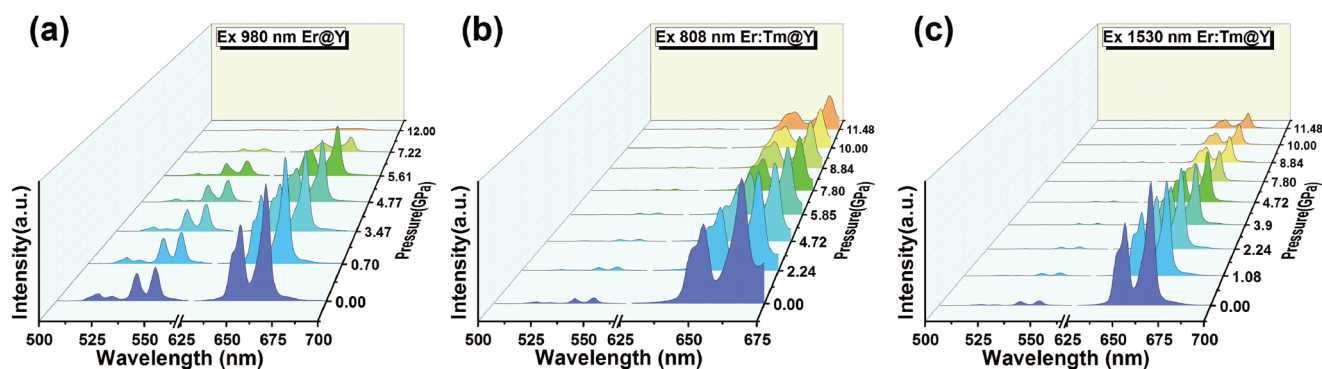


Figure 8. Pressure-response UCL spectra of a) Er@Y at 980 nm excitation (2.09 W); b) Er:Tm@Y at 808 nm excitation (1.62 W) and c) Er:Tm@Y at 1530 nm excitation (0.46 W).

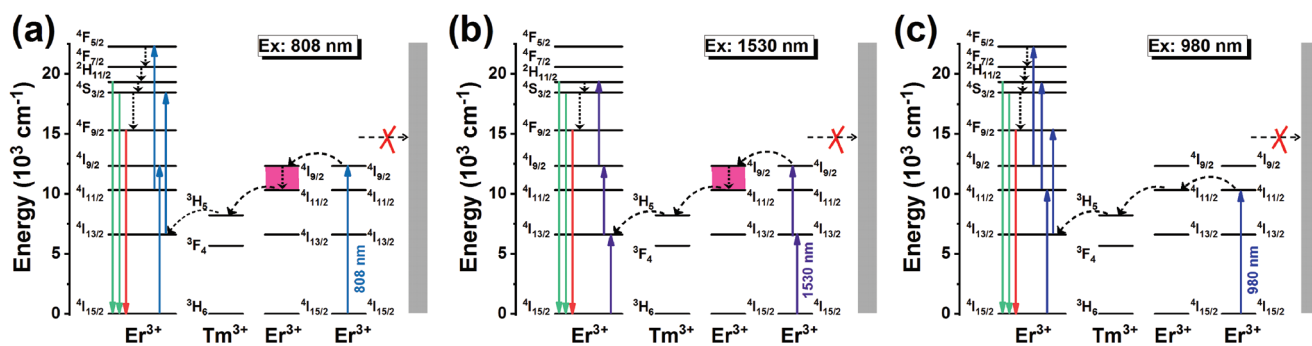


Figure 9. Proposed upconversion mechanisms for Er:Tm@Y UCNP at a) 808 nm, b) 1530 nm, and c) 980 nm excitation. The solid deep-blue (purple, light-blue), dashed black, and solid red (green) arrows represent photon excitation, energy transfer, and radiative emission, respectively.

Gd) nanoparticles achieve excitation wavelength-dependent UCL enhancement through pressure-stimulated local structural modulation. This is a very interesting and novel phenomenon, which not only provides a new research dimension for high-pressure UCL studies, but also lights the way to develop novel properties of materials through local structural engineering.

3. Conclusion

In summary, we have shown a unique excitation wavelength-dependent UCL enhancement in tetragonal phase Er:Tm@Y hosts under high pressure. With increasing pressure, the UCL peak of the Er:Tm@Y UCNP shows a continuous red shift, while the UCL intensity is only gradually enhanced only at 980 nm excitation and a maximum 2.6-fold enhancement is obtained when a pressure of ≈ 6 GPa is applied. After pressure release, the luminescence diminishes and recovers. DFT calculations show that the symmetry distortion of the LiErF_4 crystal reaches a maximum at pressurization to 6 GPa, and in addition, a new Er-4f state emerges at this time, greatly reducing the bandgap from 8.3 to 5.7 eV, verifying the experimentally observed phenomenon. Comparative experiments demonstrated that the local symmetry distortion caused by 0.5% Tm^{3+} doping and the different energy transfer patterns of Er^{3+} to Tm^{3+} at different excitations are responsible for this wavelength-dependent luminescence enhancement. The phenomena and conclusions obtained in this work deepen the understanding of the relationship between local structural engineering and optical properties of UCNP, and the selectable modulation of wavelength provides a new dimension and perspective for the study of pressure-induced UCL, which is inspiring for other similar studies.

4. Experimental Section

Materials: LiOH (98%) was bought from Aladdin. NH_4F (> 96%) was purchased from Xilong Scientific. Oleic acid (OA, 90%), 1-octadecene (ODE, 90%) and $\text{LnCl}_3 \cdot 6\text{H}_2\text{O}$ (Ln: Er, Tm, Y, Lu, Gd 99.9%) were bought from Sigma-Aldrich. All reagents were directly used without further purification.

Measurements: The powder diffraction data of UCNP were obtained via Rigaku wide-angle XRD with $\text{Cu K}\alpha$ radiation ($\lambda = 1.5406 \text{ \AA}$) in the range of 10° – 80° . The morphology and structure of UCNP were

examined by JEM-2100 transmission electron microscope (TEM). The UCL spectrum was measured by optic spectrometer (the Ocean Optics QE Pro). The positions of ruby fluorescence peaks for pressure calibration were measured by a high-resolution fiber spectrometer (Ocean Optics, HR4000). And the fluorescence lifetimes were measured by Hamamatsu R9110 PMT photon counting system as a detector.

Synthesis of Er:Tm Core Nanoparticles: The Er:Tm core UCNP were prepared by referring to the literature.^[23] $\text{TmCl}_3 \cdot 6\text{H}_2\text{O}$ (0.004 g, 0.010 mmol) and $\text{ErCl}_3 \cdot 6\text{H}_2\text{O}$ (0.760 g, 1.990 mmol) were added to a 100 mL flask with a solution of 12 mL OA and 28 mL ODE. After stirring for 30 min, the mixture was raised to 150°C for 70 min and then cooled down to 50°C . Then methanol (20 mL) dissolved with NH_4F (0.296 g, 8.000 mmol) and LiOH (0.120 g, 5.000 mmol) was added and raised to 70°C for 60 min to remove the methanol. The mixed solution was then raised to 300°C for 2 h. Next, the solution was cooled to 50°C , acetone and ethanol were added and centrifuged to obtain the core UCNP. Finally, the Er:Tm core UCNP were dispersed in 16 mL of cyclohexane for use. Note that nitrogen protection and constant stirring are required during the entire experiment.

Synthesis of Er:Tm@Ln (Ln = Y, Lu, Gd) Core-Shell Nanoparticles: $\text{LnCl}_3 \cdot 6\text{H}_2\text{O}$ (Ln: Y, Lu, Gd, 0.250 mmol) was added to a 50 mL flask with a solution of 5 mL OA and 10 mL ODE. After stirring for 30 min, the mixture was raised to 150°C for 40 min and then cooled down to 50°C . Cyclohexane (2 mL) containing Er:Tm core UCNP was added and raised to 85°C for 30 min to remove the cyclohexane, and then cooled to 50°C . Next, methanol (5 mL) dissolved with NH_4F (0.037 g, 1.000 mmol) and LiOH (0.015 g, 0.625 mmol) was added and raised to 70°C for 30 min to remove the methanol. Subsequently, the solution was raised to 300°C for 90 min ($\text{YCl}_3 \cdot 6\text{H}_2\text{O}$, 0.076 g), 200 min ($\text{LuCl}_3 \cdot 6\text{H}_2\text{O}$, 0.097 g), and 120 min ($\text{GdCl}_3 \cdot 6\text{H}_2\text{O}$, 0.093 g), respectively. Then the solution was cooled to 50°C . Next steps are the same as the synthesis of the core. Finally, the Er:Tm@Ln (Ln = Y, Lu, Gd) core-shell UCNP were dispersed in 3 mL of cyclohexane for use. Note that nitrogen protection and constant stirring are required during the entire experiment.

In Situ High-Pressure Photocurrent Measurements: A symmetric DAC with the size of 0.5 mm for producing high pressure coupled to a 980 nm laser were built for in situ UCL measurements, as shown in Scheme 1. The sample and rubies for pressure measurement are loaded into a sample chamber with silicone oil as the pressure-transmitting medium. The sample chamber was made of pre-indented type T301 stainless steel gasket (indentation, 0.07 mm; hole diameter, 0.25 mm). A fiber optic spectrometer (Ocean Optics QE Pro) was used to measure the pressure-dependent emission.

The Computational Details: The geometric and density of states (DOS) changes of LiErF_4 at different pressures (0–12 GPa) were further evaluated with DFT method to rationalize the pressure-induced effect on the UCL spectra. Due to the small response of LiYF_4 toward UCL and the extremely low doping concentration of Tm^{3+} , therefore only the LiErF_4 crystal was taken as the computational model that shown in Figure 6c. The LiErF_4 crystal represents a scheelite-type fluoride with a tetragonal crystal structure belonging to the $I4_1/a$ space group and with four

formula units per unit cell. All the DFT calculations were performed in VASP with a plane-wave basis set and projector augmented wave method by combining the PBE functional.^[35] The valence electron configurations for Er, Li, and F were $4f^{11}5s^25p^66s^25d^1$, $1s^22s^1$, and $2s^22p^5$, respectively. To consider the strong correlation effects of 4f-electrons in the rare-earth Er ion, the GGA is carried out with an onsite Coulomb repulsion parameter U of 7.6 eV.^[36] The unit cell lattice constants and ionic positions were fully relaxed at different pressures until self-consistency with thresholds of 1×10^{-6} eV and 2×10^{-2} eV Å⁻¹ for electronic and ionic convergence, respectively. The kinetic energy cutoff is set to 500 eV. Brillouin zone is integrated with Γ -centered $10 \times 10 \times 5$ and $13 \times 13 \times 6$ k-point mesh in the reciprocal space of the unit cell during optimization and density of states calculations, respectively.

Supporting Information

Supporting Information is available from the Wiley Online Library or from the author.

Acknowledgements

This work was financially supported by the National Natural Science Foundation of China (Nos. 61875191, U2003127, 62171194, 11874355, and 21902057). Natural Science Foundation of Jilin Province (20210101380JC).

Conflict of Interest

The authors declare no conflict of interest.

Data Availability Statement

The data that support the findings of this study are available from the corresponding author upon reasonable request.

Keywords

excitation wavelength-dependent, $\text{LiErF}_4:0.5\%\text{Tm}^{3+}/\text{LiYF}_4$, local structural engineering, high pressure, upconversion enhancement

Received: December 2, 2022

Revised: February 3, 2023

Published online: March 22, 2023

- [1] X. Guo, Y. Yuan, J. Liu, S. Fu, J. Zhang, Q. Mei, Y. Zhang, *Anal. Chem.* **2021**, 93, 3010.
- [2] Z. M. Zhang, S. Shikha, J. L. Liu, J. Zhang, Q. S. Mei, Y. Zhang, *Anal. Chem.* **2019**, 91, 548.
- [3] T. Jia, Q. Wang, M. Xu, W. Yuan, W. Feng, F. Li, *Chem. Commun.* **2021**, 57, 1518.
- [4] M. Huo, P. Liu, L. Zhang, C. Wei, L. Wang, Y. Chen, J. Shi, *Adv. Funct. Mater.* **2021**, 31, 2010196.

- [5] G. Xiang, Q. Xia, X. Liu, Y. Wang, S. Jiang, L. Li, X. Zhou, L. Ma, X. Wang, J. Zhang, *Nanoscale* **2021**, 13, 7161.
- [6] M. Xu, B. Xue, Y. Wang, D. Wang, D. Gao, S. Yang, Q. Zhao, C. Zhou, S. Ruan, Z. Yuan, *Small* **2021**, 17, 2101397.
- [7] B. S. Richards, D. Hudry, D. Busko, A. Turshatov, I. A. Howard, *Chem. Rev.* **2021**, 121, 9165.
- [8] Q. Zhang, J. Deng, Z. Xu, M. Chaker, D. Ma, *ACS Catal.* **2017**, 7, 6225.
- [9] C. Homann, L. Krukewitt, F. Frenzel, B. Grauel, C. Wurth, U. Resch-Genger, M. Haase, *Angew. Chem.* **2018**, 57, 8765.
- [10] S. Liu, Z. An, J. Huang, B. Zhou, *Nano Res.* **2023**, 16, 1626.
- [11] S. Liu, L. Yan, J. Huang, Q. Zhang, B. Zhou, *Chem. Soc. Rev.* **2022**, 51, 1729.
- [12] H. Dong, L. D. Sun, C. H. Yan, *J. Am. Chem. Soc.* **2021**, 143, 20546.
- [13] S. B. Liu, Z. C. An, B. Zhou, *Chem. Eng. J.* **2023**, 452, 139649.
- [14] L. Wang, H. Dong, Y. Li, C. Xue, L. D. Sun, C. H. Yan, Q. Li, *J. Am. Chem. Soc.* **2014**, 136, 4480.
- [15] J. Lee, B. Yoo, H. Lee, G. D. Cha, H. S. Lee, Y. Cho, S. Y. Kim, H. Seo, W. Lee, D. Son, M. Kang, H. M. Kim, Y. I. Park, T. Hyeon, D. H. Kim, *Adv. Mater.* **2017**, 29, 201603169.
- [16] Z. Yin, H. Li, W. Xu, S. Cui, D. Zhou, X. Chen, Y. Zhu, G. Qin, H. Song, *Adv. Mater.* **2016**, 28, 2518.
- [17] M. Runowski, J. Marciniak, T. Grzyb, D. Przybylska, A. Shyichuk, B. Barszcz, A. Katrusiak, S. Lis, *Nanoscale* **2017**, 9, 16030.
- [18] S. Mei, Y. Guo, X. Lin, H. Dong, L. D. Sun, K. Li, C. H. Yan, *J. Phys. Chem. Lett.* **2020**, 11, 3515.
- [19] H. Bao, W. Wang, X. Li, X. Liu, L. Zhang, X. Yan, Y. Wang, C. Wang, X. Jia, P. Sun, X. Kong, H. Zhang, G. Lu, *Adv. Opt. Mater.* **2021**, 10, 2101702.
- [20] A. Lay, D. S. Wang, M. D. Wisser, R. D. Mehlenbacher, Y. Lin, M. B. Goodman, W. L. Mao, J. A. Dionne, *Nano Lett.* **2017**, 17, 4172.
- [21] M. D. Wisser, M. Chea, Y. Lin, D. M. Wu, W. L. Mao, A. Salles, J. A. Dionne, *Nano Lett.* **2015**, 15, 1891.
- [22] K. Zhang, C. Gao, Z. Jiang, Y. Wei, Y. Pan, C. Wei, H. Li, K. Wang, B. Zou, L. Huang, *Adv. Opt. Mater.* **2019**, 8, 1901031.
- [23] Z. Li, Y. Zhang, *Nanotechnology* **2008**, 19, 345606.
- [24] L. Zhang, X. Li, W. Wang, X. Zhao, X. Yan, C. Wang, H. Bao, Y. Lu, X. Kong, F. Liu, X. Liu, G. Lu, *Nano Res.* **2020**, 13, 2803.
- [25] J. Zuo, Q. Q. Li, B. Xue, C. X. Li, Y. L. Chang, Y. L. Zhang, X. M. Liu, L. P. Tu, H. Zhang, X. G. Kong, *Nanoscale* **2017**, 9, 7941.
- [26] Q. Chen, X. Xie, B. Huang, L. Liang, S. Han, Z. Yi, Y. Wang, Y. Li, D. Fan, L. Huang, X. Liu, *Angew. Chem.* **2017**, 56, 7605.
- [27] C. Zhang, J. Y. Lee, *ACS Nano* **2013**, 7, 4393.
- [28] N. J. Johnson, F. C. van Veggel, *ACS Nano* **2014**, 8, 10517.
- [29] A. Lay, C. Siefel, S. Fischer, R. D. Mehlenbacher, F. Ke, W. L. Mao, A. P. Alivisatos, M. B. Goodman, J. A. Dionne, *Nano Lett.* **2018**, 18, 4454.
- [30] W. Wang, Z. Feng, B. Li, Y. Chang, X. Li, X. Yan, R. Chen, X. Yu, H. Zhao, G. Lu, X. Kong, J. Qian, X. Liu, *J. Mater. Chem. B* **2021**, 9, 2899.
- [31] P. Woźny, M. Runowski, S. Lis, *J. Lumin.* **2019**, 209, 321.
- [32] R. E. Thoma, C. F. Weaver, H. A. Friedman, H. Insley, L. A. Harris, H. A. Yakel, *J. Phys. Chem.* **1961**, 65, 1096.
- [33] S. A. Miller, H. E. Rast, H. H. Caspers, *J. Chem. Phys.* **1970**, 52, 4172.
- [34] S. P. S. Porto, J. F. Scott, *Phys. Rev.* **1967**, 157, 716.
- [35] G. Kresse, J. Furthmüller, *Phys. Rev. B* **1996**, 54, 11169.
- [36] S. Sanna, W. G. Schmidt, T. Frauenheim, U. Gerstmann, *Phys. Rev. B* **2009**, 80, 104120.